45th AIAA/ASME/SAE/ASEE Joint Propulsion Conference & Exhibit
2 - 5 August 2009, Denver, Colorado

AIAA 2009-5366

An Unexamined Collision-less Mechanism for Electron Mobility in Hall Thrusters

Emily C. Fossum* and Lyon B. King†
Michigan Technological University, Houghton, MI, 49931, USA

This paper presents the observation of an electron mobility mechanism in Hall thruster fields that cannot be described using the theories of classical mobility or Bohm mobility, where this mobility was observed in the Hall Electron Mobility Gage, a device dedicated to investigating electron mobility. The mechanisms most commonly cited for enhanced electron mobility in Hall thrusters— collisions with dielectric walls and self-sustained plasma oscillations— have been removed, yet the mobility observed in this device fails to exhibit a magnitude agreeing with the classical prediction. The magnitude of the experimental mobility falls between the predictions of classical and Bohm mobility (Bohm coefficient of 1/16) and exhibits behavior that suggests the presence of both a collisional and collisionless mechanism for mobility. This collisionless mechanism has not yet been identified.

Nomenclature

Subscripts

B, B	Magnetic field vector, magnitude
E, E	Electric field vector, magnitude
$\bar{\epsilon}_i$	Average energy change per collision
J_a	Current density at the anode of the Hall Electron Mobility Gage
J_p	Probe current density
λ_D	Debye length
μ_{ez}	Axial mobility in the Hall Electron Mobility Gage
n_∞	Electron density in absence of the Langmuir probe
ν_i	Ionization collision frequency
ν_m	Momentum transfer collision frequency
ω_{ce}	Cyclotron frequency
$\bar{v}_e$	Average electron velocity

I. Introduction

Hall thrusters are highly-efficient in-space propulsion devices that utilize an electric field via a positively charge anode to accelerate propellant ions from the spacecraft producing thrust[1]. Electrons are attracted to the anode, and without some mechanism to retard the electron motion, the electron current would create a "short circuit" eliminating the thrust mechanism. Therefore, a magnetic field is applied transverse to the electric field which serves to "magnetize" electrons in gyro-orbits and their motion toward the anode is significantly impeded. The electron velocity toward the anode can be described by

$$u_{ez} = \mu_{ez} E_z \tag{1}$$

*NRC Research Associate, AFRL, Munitions Directorate, Eglin AFB, FL, AIAA Student Member.
†Associate Professor, Mechanical Engineering, 815 R. L. Smith Bldg. 1400 Townsend Dr. Houghton, MI 49930

where u_{ez} is the cross-magnetic-field velocity with the magnetic field in the radial direction, E_{ez} is the accelerating axial electric field, and μ_{ez} is the cross-field mobility, which is defined as the constant of proportionality between the velocity and electric field. Classical mobility describes the mechanism whereby collisions allow electrons to cross the magnetic field. The classical mobility (given magnetized electrons) is given by

$$\mu_{ez} = \frac{\nu_m}{\omega_{ce} B_r} \tag{2}$$

Electron mobility in Hall thrusters has been experimentally found to be much greater than can be described by classical collisional transport theory[2, 3]. Furthermore, the experimentally observed electron mobility in Hall thrusters is not adequately captured by any currently known theory as the underlying physics is complex and not fully understood. Excessive electron mobility stands as an efficiency loss mechanism in Hall thrusters, as an increase in electron current provides no increase in thrust[4, 5]. The poor understanding of electron mobility in Hall thrusters also limits computational modeling for prediction of discharge parameters and failure mechanisms. Because of the lack of understanding, empirical data from experiments has historically been used in modeling codes[6, 7, 8, 9, 10], which limits the ability to model new Hall thruster geometries without first obtaining experimental measurements.

The two most cited contributors to electron mobility in Hall thrusters are collisions with dielectric walls[11, 12, 13] and fluctuation-induced mobility[14, 15, 16, 17, 18]. The main difficulty in studying electron transport in Hall thrusters is the coupling that exists between the plasma and the fields, where the plasma creates and yet is influenced by the electric field. Furthermore, the electric and magnetic fields are internally coupled, where the shape and strength of the magnetic field directly influences the electric field and these parameters cannot be independently varied. Likewise, the neutral (propellant) density directly influences several discharge properties of the Hall thruster, where changes in neutral density cannot be investigated for a direct effect on electron mobility. The difficulty becomes compounded when considering wall effects and fluctuations. For example, the interaction at the dielectric wall has been hypothesized to contribute to instabilities, leading to transport, which changes the field structure at the dielectric walls. Likewise, fluctuations arise out of the field conditions, which contribute to transport, which changes the field conditions. The theory of Bohm is given by

$$\mu_{Bohm} = \frac{1}{16B} \tag{3}$$

which was determined empirically to describe the mobility arising out of fluctuations[19, 20]. Although Bohm mobility may be on the same order of magnitude as the mobility found in a Hall thruster[3], the theory falls short in describing the mobility over the length of the Hall thruster discharge channel. Attempts have been made at a closed form solution of fluctuation-induced mobility[16, 21], and although these attempts show promise, they have yet to produce results that agree with experiments. A number of investigations are ongoing to experimentally, computationally or theoretically study electron mobility in Hall thrusters[21, 22, 23, 8, 24].

A device has been constructed at MTU's Isp Lab, the Hall Electron Mobility Gage, which was designed specifically to study electron transport in Hall thruster fields, where the coupling between the parameters of electric field, magnetic field and neutral density has been virtually eliminated. Also, in this device the two most cited contributors to electron transport in Hall thrusters, fluctuation-induced transport and wall effects, have been removed. The dielectric walls were physically removed and radial confinement was achieved through electric and magnetic fields, where the confinement properties were presented elsewhere[25]. The electron density was limited to 10^9 to 10^{11} m^{-3}, and electron temperatures were found to be 10-30 eV, resulting in a Debye length much greater than apparatus dimensions ($\lambda_D \sim 1$ m). According to Pines and Bohm, collective plasma oscillations cannot be sustained on length scales small compared to the Debye length[26], and consequently, self-sustained plasma fluctuations hypothesized to contribute to mobility in Hall thrusters, theoretically cannot exist in the Mobility Gage.

Removing the dielectric walls and plasma fluctuations, while maintaining the field environment in vacuum, has allowed the study of electron dynamics in Hall thruster fields where the electrons behave as test particles in prescribed fields, greatly simplifying the environment. Therefore, it was possible to observe any effects on transport not linked to the cited mechanisms, and it was possible to observe trends of the enhanced mobility with control parameters of electric and magnetic fields and neutral density– parameters that are not independently variable in a Hall thruster. A schematic of the Hall Electron Mobility Gage is shown in Fig. 1, where a detailed description of the design, construction and setup is described elsewhere[27, 28].

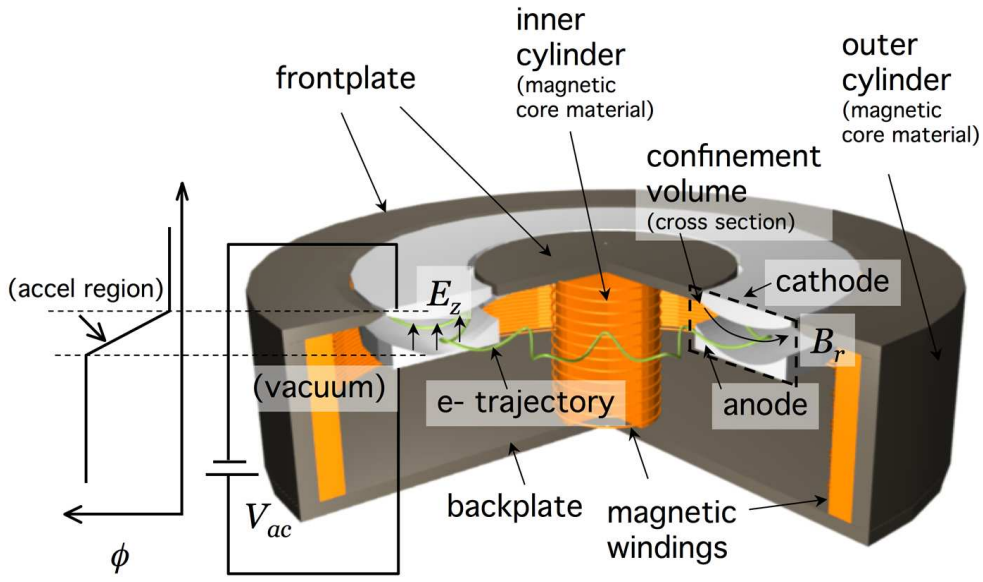

Figure 1. Schematic of the defining features of the Hall Electron Mobility Gage including electric field creation and resulting potential (qualitative).

II. Experimental Setup and Methods

The experimental setup used for mobility measurements described in this paper was reported on in Ref. [28], and only a brief description will be presented here. Figures 2 and 3 show the experimental setup used to measure mobility within the Hall Electron Mobility Gage. The Mobility Gage was operated in the Isp Lab Vacuum Test Facility #2, a 2-m-diameter, 4-m-long cylindrical vacuum chamber. Rough pumping was accomplished through a two-stage mechanical pump, capable of delivering 400 cfm. High vacuum was achieved through the use of three turbomolecular pumps with a combined throughput of 6,000 liters per second providing a base pressure below 10^{-6} Torr. All experiments presented herein were conducted within this facility.

An ion gage (shown in Figs. 2 and 3) was mounted directly to the Mobility Gage in order to obtain a local measure of pressure inside the Mobility Gage. Background gas (argon) was introduced directly into the vacuum tank (inlet shown in Fig. 2) where gas flow was controlled through mass flow controllers (shown in Fig. 2) to vary the base pressure from 10^{-6} to 10^{-4} Torr. The magnetic and electric fields (Fig. 3) were created through magnetic windings and parallel plates, respectively, where the electrical schematics for both are shown. The inner and outer magnetic coils were supplied by independently controlled Sorensen DLM60-10 power supplies operated in current-limited mode. The current directions for the inner and outer coils are shown in Fig. 3, as well. The shape and strength of the magnetic field was determined using a numerical magnetic field solver, Maxwell SV[29], and verified using experimental measurements with a Gauss probe. The electric field was created using a Sorensen DHP600 programmable power supply and 390 μF filtering capacitors were employed, as shown, to dampen oscillations in the power supply voltage. The electric equipotential structure and electric field strength were also determined using the vacuum solution of Maxwell SV[29] since the plasma contribution was deemed negligible due to the low electron density and long Debye length. The resulting electric equipotentials and magnetic field lines are shown in Fig. 4. The experimental setup and methods for calibration and control are described in more detail elsewhere[28]. This experimental setup allows for independent control of the electric and magnetic fields and pressure, which is not possible in a Hall thruster.

Electrons were loaded into the Mobility Gage using a thermionic emitting filament shown in Fig. 3 by resistively heating the filament with current, I_h and biasing the filament to voltage, V_f, controlled through

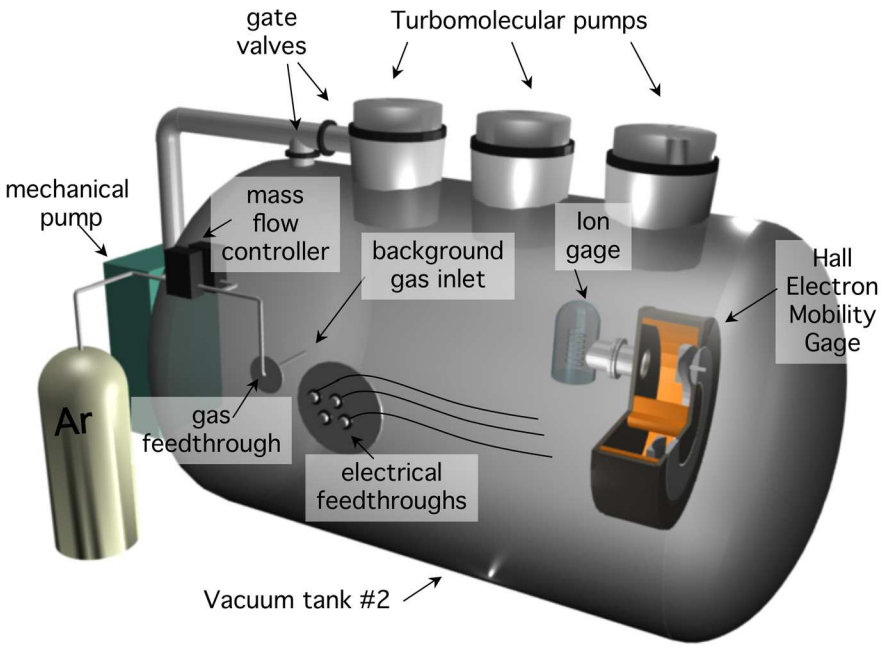

Figure 2. Experimental setup and electrical schematic for the Hall Electron Mobility Gage.

a variable resistance voltage divider, as shown. The emission current, I_e, was controlled through control of I_h, which provided a control of electron density within the confinement volume. The emission filament supplied the confinement volume with electrons, where electrons filled the confinement volume by assuming an azimuthal $\mathbf{E} \times \mathbf{B}$ drift over the channel annulus and traversing the confinement volume by axial mobility. The electrons were collected at the anode, and electron current was measured with a Femto DLPCA200 variable-gain, low-noise current amplifier.

Mobility is given by Eq. 1, where μ_{ez} is defined as the constant of proportionality between the cross-field velocity of electrons and the electric field orthogonal to the magnetic field. In the Hall Electron Mobility Gage the electric field is known from the numerical solution of the vacuum electrostatic configuration because the electron density is sufficiently low and Debye length sufficiently long that the field can be assumed rigid. Therefore, only a measurement of the axial velocity was necessary to determine the mobility. A measurement of current at the anode (with known area, $A_a = 0.099$ m^2) provided a measure of the axial current density, $J_a = I_a/A_a$, which, given a measurement of electron density, provided the axial velocity, where

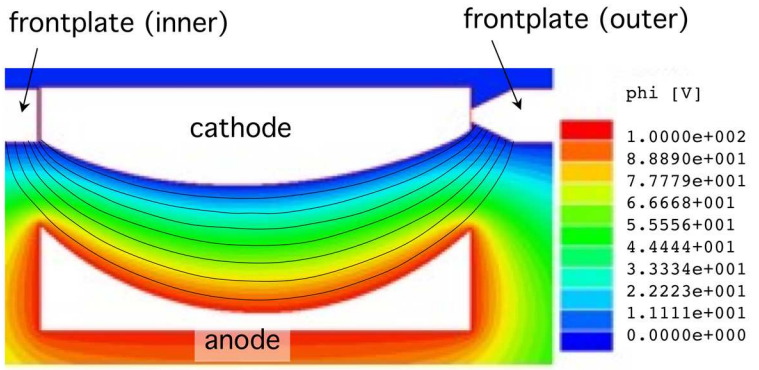

Figure 4. Contour plot of electrostatic equipotentials (color) with magnetic field lines (solid black) superimposed.

$$u_{ez} = \frac{J_a}{qn_e} \tag{4}$$

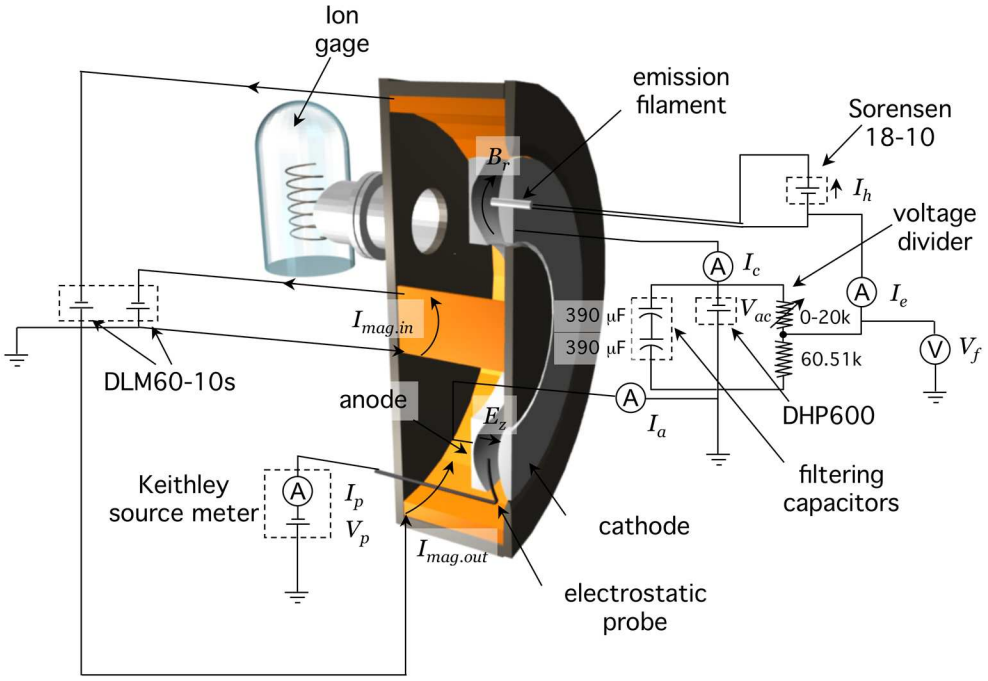

Figure 3. Experimental setup and electrical schematic for the Hall Electron Mobility Gage.

Electron density was measured using a planar electrostatic Langmuir probe with collection area ($A_p = 4.4 \times 10^{-6}$ m^2) normal to the magnetic field, and thus normal to the bulk $\mathbf{E} \times \mathbf{B}$ drift. Thus, the probe was sensitive only to electron thermal velocity parallel to the magnetic field. A curve fit to an I-V probe characteristic provided the experimental measure of electron density, where the probe current density may be expressed by

$$J_p = \frac{1}{4} e n_\infty \bar{v}_e \exp(V_0) \tag{5}$$

The electron density, n_∞, represents the electron density in absence of the probe, $\bar{v}_e$ is the average electron velocity given by $\sqrt{8kT_e/\pi m_e}$, and $V_0 = -e(V_p - \phi_{local})/kT_e$. The curve fit for electron density also provided a measurement of electron temperature. A more thorough description of this method is provided in Refs. [28] and [27].

The cross-field mobility was evaluated experimentally by combining the result of the probe I-V characteristic with the axial (anode) current so that

$$\mu_{ez} = \frac{J_a}{E_z q n_e} \tag{6}$$

This measurement technique provided a measurement of axial mobility at the location of the probe assuming constant axial electron flux ($J_a = J_{ez}$) from the probe to the anode. Non-constant axial electron flux due to ionizing collisions that take place in the axial distance between the probe and the anode were accounted for using the methods presented in Ref. [28], although this correction was relatively small and fell within the realm of experimental uncertainty of other measured parameters. Mobility was examined in response to the control parameters of electric field, magnetic field and pressure and the results are presented in Section III. Each of these control parameters was varied independently in order to investigate trends of the experimental mobility over the range of each control parameter.

Calculations for classical and Bohm mobility were needed for comparison with experimental mobility. Classical (cross-field) mobility is given in Eq. 2 in the case of high Hall parameter. For the calculation

of classical mobility an estimation of momentum-transfer collision frequency and the magnetic field were needed. The magnetic field strength was determined from the Maxwell SV[29] numerical solutions, which were validated through experimental measurements of the magnetic field using a Gauss probe. The momentum transfer collision frequency was calculated based on the electron-neutral collision frequency, since Coulomb collisions were deemed negligible due to the low electron density combined with high average electron velocity. The electron-neutral collision frequency is given by $\nu_{en} = n_0 \sigma \bar{v}_e$ where n_0 is the neutral density, σ is the collision cross-section and $\bar{v}_e$ is the average electron velocity. The neutral density was calculated using the ideal gas law given by $n_0 = p/(RT)$, based on the pressure measured with the B-A type ion gage. The electron velocity was determined from the measured electron temperature (from the electrostatic probe) and given as the average velocity of a Maxwellian distribution, $\bar{v}_e = \sqrt{8kT_e/\pi m_e}$. The electron-neutral collision cross section was estimated from the cross-section data provided in the Siglo database[30]. The cross section was found based on the electron energy given by $3kT_e/2$, where the electron temperature was given by the experimentally measured value. Bohm mobility was calculated using the same magnetic field as in the case for classical mobility and is given by Eq. 3.

III. Results and Analysis

III.A. Mobility Results

Mobility is defined as the constant of proportionality between axial velocity and electric field. To examine this relationship mobility was examined in response to electric field, where a sample of the results are shown in Fig. 5[a]. There is no statistically significant difference in mobility over the electric field range examined as any changes in mobility fall within the realm of experimental error. This result indicates that the axial cross-field velocity of electrons increases proportionally with the electric field which is expected by both theories of classical and Bohm mobility. However, the order of magnitude of the experimental mobility falls between the values of Bohm and classical mobility.

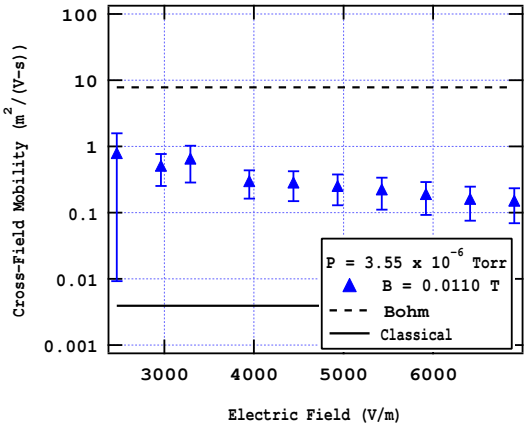

Figure 5. Sample sweep of experimental mobility versus electric field for a constant magnetic field and pressure. Classical and Bohm mobility are included for comparison.

Mobility was examined in response to magnetic field for nine conditions of electric field and pressure, where the results are presented in the Appendix, Fig. 9. A sample sweep is shown in Fig. 6. These results show a statistically significant decrease in mobility with magnetic field. Classical mobility scales as B^{-2} and Bohm mobility scales as B^{-1}. If the coefficients for Bohm and classical mobility were relaxed, a curve fit with scaling, B^{-2} and B^{-1}, may be fit to the experimental data. In other words, a constant C_1 and C_2 may be used to fit the experimental data to the relations $\mu_{exp} = C_1 \mu_{Class}$ and $\mu_{exp} = C_2 \mu_{Bohm}$. The curve fits are shown in Fig. 6, showing that the scaling with B cannot be resolved over the range of magnetic fields explored where B^{-2} and B^{-1} scaling both fit within the realm of experimental error. The curve fit for the data in Fig. 6 using classical scaling is represented by $\mu_{exp} = 25\mu_{Class}$. The curve fit for the data using Bohm scaling is represented by $\mu_{exp} = 0.04\mu_{Bohm}$, or equivalently, the Bohm coefficient of 1/16 is replaced by a coefficient of 1/400 (i.e. $\mu_{exp} = 1/(400B)$). Looking at the data in Fig. 9 (Appendix), it appears that the B^{-2} curve fit for the low pressure conditions provides a better fit, where the B^{-1} curve fit for the high pressure conditions provides a better fit. However, this is purely speculative as both curve fits lie within the realm of experimental error for almost all conditions.

Mobility was examined in response to pressure for nine conditions of electric field and magnetic field, where an increase in experimental mobility with pressure was statistically significant. The results are presented in Fig. 10 and a sample sweep is shown in Fig. 7. Again, if the coefficient for mobility were relaxed and the

[a]Error bars are presented for all experimental data that reflect the error introduced by the quality of the curve fit for T_e and n_e, the variance in pressure measurements, the variance in the measurement of anode current and the estimated error due to the non-constant axial flux between the probe and the anode. The greatest source of error is due to the quality of the curve fit for T_e and n_e where the error was determined from the covariance matrix of the least-squares curve fit.

classical scaling with pressure were imposed, the curve fit shows $\mu_{exp} = 50\mu_{Class}$. If a collisionless mechanism were included the curve fit shows $\mu_{exp} = 25\mu_{Class} + 0.2$. These curve fits are shown in Fig. 7. The constant may also be expressed as a fraction of Bohm mobility since Bohm mobility is independent of pressure. This would be given by $mu_{exp} = 25\mu_{Class} + 0.03\mu_{Bohm}$. The curve fit with the collisionless component seems to fit the data better; however, this trend cannot be confirmed without extending the range of pressure significantly lower.

In nearly all cases the experimental mobility fell between Bohm mobility and classical mobility. While errors in the classically predicted mobility coefficient may arise out of errors in pressure measurement, electron temperature measurement, or the momentum-transfer cross section for electron collisions with argon, it is highly unlikely that these errors can account for the discrepancy between classical and experimental, varying by a factor of 20 to 100. Curiously, the experimental mobility shows signs of classical trends— that is a decrease in mobility with magnetic field and an increase in mobility with pressure. Despite these trends, it has been determined that the experimental mobility cannot be accounted for by collisions alone and another mechanism, independent of collisions, is present in the Hall Electron Mobility Gage.

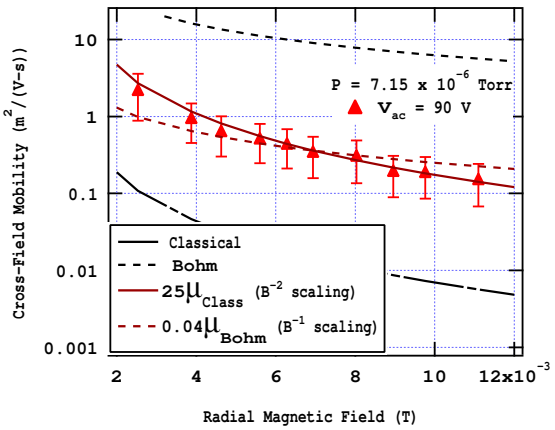

Figure 6. Sample sweep of experimental mobility versus magnetic field for a constant electric field and pressure. Classical and Bohm mobility are included for comparison and a curve fit scaling as B^{-2} and scaling as B^{-1} are shown.

It is notable that the two most cited contributors to mobility in Hall thrusters, wall collisions and self-sustained plasma oscillations and/or turbulence, cannot be present in the Hall Electron Mobility Gage. Therefore, some other mechanism for mobility must be present in the Mobility Gage that does not depend on collisions, which may also be present in a Hall thruster. The magnitude of Hall thruster mobility generally falls on the same order of magnitude as Bohm mobility**??**, which is at least an order of magnitude higher than the mobility observed in this device. Therefore, these findings do not negate the possibility of either or both wall collisions and fluctuations contributing to mobility in a Hall thruster. However, these findings do point to a collisionless mechanism in absence of these, which may also be present in a Hall thruster, that has not been previously isolated or observed.

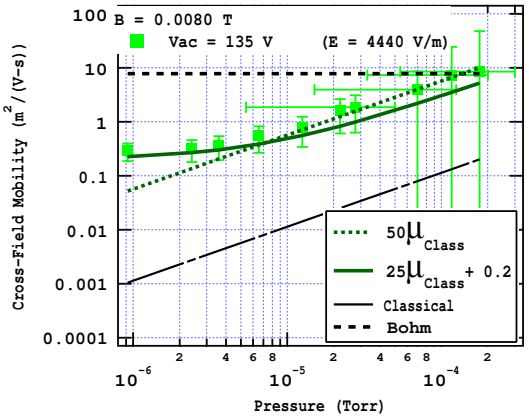

Figure 7. Sample sweep of experimental mobility versus pressure for a constant electric field and magnetic field. Classical and Bohm mobility are included for comparison. A curve fit with classical scaling ($\mu_{exp} = C_1\mu_{Class}$) and a curve fit with an collisionless component $\mu_{exp} = C_1\mu_{Class} + C_2$ are shown.

III.B. Support for Collisionless Mobility

Measurements of electron temperature with variations in pressure in the Hall Electron Mobility Gage have been previously presented[27]. Electron temperature was found to decrease with increasing pressure, where

this trend was postulated to arise out of a collisionless mechanism for electron mobility. An argument may be made that, given purely classical mobility, the axial profile of electron energy should be unchanging with neutral density (pressure), where energy and temperature are directly related[31]; conversely, if electron temperature (which should be constant with axial distance and electric/magnetic field conditions) were found to vary with neutral density, a non-classical transport mechanism was present that was not dependent on electron-neutral collisions. Assuming electrons are magnetized (large Hall parameter), for classical collision-driven mobility the number of total collisions required to traverse a given distance across the magnetic field is fixed by the field conditions, regardless of how often collisions take place. At constant electric field, the total energy available to electrons is fixed as well. Electrons lose a certain amount of energy through inelastic collisions with neutrals, which is dependent on incident electron energy, where incident energy is governed by the energy gained from the electric field, and thus energy losses are also fixed by the field conditions. Therefore, the net energy change for electrons as they traverse the confinement volume axially should be independent of collision frequency, since both the total number of collisions and the energy gain and loss for an electron moving through the confinement volume are fixed by the field conditions. In other words, the collision frequency would only affect the total residence time of electrons in the trap (or equivalently axial velocity, u_{ez}), but collision frequency would not affect the total energy gain and collisional cooling effects as an electron traverses from the loading filament to the anode. (In the limit of complete vacuum where collision frequency is zero, an electron will not move through the confinement volume and will remain indefinitely in an azimuthal $\mathbf{E} \times \mathbf{B}$ orbit.) Therefore, if collisions are solely responsible for cross-field mobility, the axial profile of electron temperature (or equivalently, the electron temperature at a given axial location) will be constant with collision frequency and hence neutral density.

In the case of collisionless or anomalous mobility, electron temperature could be dependent on electron-neutral collision frequency. To illustrate this, consider a mechanism for cross-field electron mobility that allows electrons to move across the field in complete absence of neutrals (vacuum condition). The time-of-flight required to travel from cathode-to-anode would be finite regardless of collision frequency (in contrast to collisional mobility where time-of-flight would be infinite in the absence of collisions). The presence of neutrals would, however, affect the temperature of the electrons because of collisional cooling; the degree to which electrons are cooled depends on the number of collisions an electron encounters while moving through the confinement volume. In the limit of absolute vacuum an electron experiences no collisions and gains the maximum amount of energy from the field, displaying a high electron temperature. In the case of low neutral density, electrons are cooled as they suffer collisions during their journey; as neutral density increases the amount of "cooling" would increase, showing a decrease in T_e as n_0 is increased.

Figure 8 shows measured a sample sweep of electron temperature versus neutral density where a statistically significant decrease in temperature is evident with increasing pressure. It follows then that the observed variation of electron temperature with neutral density is consistent with a mobility mechanism that does not require electron-neutral collisions.

This type of electron temperature investigation (i.e. determining the type of mobility based on analysis of electron temperature) is illustrated eloquently by Levchenko[23] in the derivation of an electron energy equation for classical and Bohm mobility. This equation accounts for energy gain from the electric field and energy losses due to ionizing collisions. Here the equations are adapted from Levchenko to reflect both the nomenclature used throughout this paper and the geometry of the Hall Electron Mobility Gage (axial E, radial B). The change in electron thermal energy (of an electron population) is given by

$$\frac{\partial \epsilon_e}{\partial z} = E_z - \psi_e \bar{\epsilon}_i \tag{7}$$

where E_z is the axial rate of energy gain due to the electric field, $\psi_e \bar{\epsilon}_i$ is the energy loss per distance traveled and ϵ_i is the energy change (loss) per collision (in Levchenko[23] this energy loss accounts for both the ionization energy loss from the incident electron and the addition of the "born" electron in the electron energy distribution with energy equivalent to the neutral density, i.e. very low energy). The energy loss per distance traveled ($\psi_e \bar{\epsilon}_i$) may be expressed as

$$\psi_e \bar{\epsilon}_i = \frac{\nu_i \bar{\epsilon}_i}{u_{ez}} \tag{8}$$

where ν_i is the ionization collision frequency given by

$$\nu_i \;=\; n_0 \left\langle \sigma_{ion} v_e \right\rangle \;=\; n_0 \int_0^\infty \sigma_i(v_e) v_e f(v_e) dv_e \tag{9}$$

and u_{ez} may be found using the mobility coefficient and electric field (Eq. 1). Substituting the classical mobility coefficient and the Bohm mobility coefficient (Eq. 2 and 3, respectively) results in Equations 10 and 11:

$$\frac{\partial \epsilon_e}{\partial z} \;=\; E_z - \frac{e}{m_e}\frac{\sigma_i}{\sigma_m}\frac{B_r^2}{E_z}\bar{\epsilon}_i \tag{10}$$

$$\frac{\partial \epsilon_e}{\partial z} \;=\; E_z - n_0 \sigma_i \bar{v}_e \frac{16 B_r}{E_z}\bar{\epsilon}_i \tag{11}$$

(the constant cross-section approximation has been made in these equations, which does not have any consequence on the main point of presenting these equations—it only removes an integral so it is more convenient to write)

Within these equations it is apparent that the energy in the classical solution is not dependent on neutral density; however, the energy in the equation solved using the Bohm mobility coefficient retains a dependence on neutral density. Equation 11 would retain the dependence on neutral density for any collisionless mobility mechanism, where in the general case the energy equation is given by

$$\frac{\partial \epsilon_e}{\partial z} \;=\; E_z - \frac{n_0 \sigma_i \bar{v}_e}{\mu_{ez} E_z}\bar{\epsilon}_i \tag{12}$$

A numerical model was employed to determine the classical and Bohm electron energy (and thus electron temperature where $E_e = 3kT_e/2$) for the Hall Electron Mobility Gage, based on the energy analysis by Levchenko. In this analysis, electrons born out of ionizing collisions were given an energy of 0.1 eV[32] and the total energy was recalculated incorporating the "born" electrons into the distribution. The constant cross-section approximation was used where the average energy per step was used to determine the corresponding momentum-transfer and ionization cross sections. A sample plot of T_e versus pressure is shown in Fig. 8. The results to the classical and Bohm models for electron temperature with pressure are shown as solid and dashed (black) lines, respectively in Fig. 8.

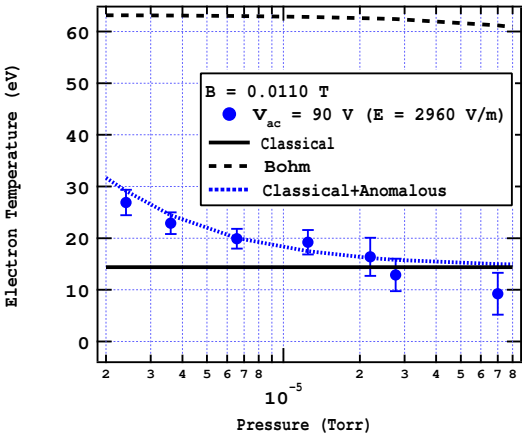

Figure 8. Sample sweep of experimental mobility versus pressure for a constant electric field and magnetic field. Classical and Bohm mobility are included for comparison. A curve fit with classical scaling ($\mu = C_1 P^{1.0}$) and a curve fit with an collisionless component $\mu = C_1 P^{1.0} + C_2$ are shown.

The electron temperatures calculated using the Bohm mobility model were much higher than measured values. However, given the order of magnitude of the experimental mobility, which was always less than the Bohm mobility, it was suspected that the Bohm model overestimated the axial velocity (and thus energy gain) so the disagreement was not unexpected. Adapting the analysis shown above (Eq. 12), a third model was applied presenting an anomalous mobility constant in addition to the classical mobility, which varies with neither B nor pressure and is given as a constant of $\mu_{AN} = 0.005$[b]. The energy equation in this case is given by

$$\frac{\partial \epsilon_e}{\partial z} \;=\; E_z - \frac{n_0 \sigma_i \bar{v}_e}{(\mu_c + \mu_{AN}) E_z}\bar{\epsilon}_i \tag{13}$$

This analysis (of μ_{AN}) is in no way meant to be exhaustive, but is presented only to qualitatively examine the effects of a constant "axial leakage current" that allows electrons to traverse from anode to cathode in absence of collisions, which could dominate at low pressures. The results of this analysis are also presented in Fig. 8.

[b]The choice of the value of $\mu_{AN} = 0.005$ was largely arbitrary. The only justification for using this value is that under higher pressure conditions, the classical mobility dominates ($\mu_{class} > 0.005$) and under the lowest pressure conditions, the anomalous mobility dominates ($\mu_{class} < 0.005$).

The trends captured by the "axial leakage current" model at least qualitatively agree with what is observed, particularly concerning the variation of electron temperature with pressure. Although the classical model for electron temperature is not far outside the realm of experimental error, the trend of electron temperature with pressure is more fully captured with the "axial leakage current" model. This provides corroborating evidence for a collisionless mobility mechanism in light of the mobility measurements obtained. These results are encouraging and give credence to the existence of a collisionless mechanism contributing to the overall mobility in the Hall Electron Mobility Gage.

IV. Conclusions

Non-classical mobility was exhibited in the Hall Electron Mobility Gage, a device dedicated to mobility studies in the field conditions of a Hall thruster. Non-classical mobility in Hall thrusters has been hypothesized to be due to electron collisions with dielectric walls and plasma oscillations and/or turbulence, both of which have been shown to be absent in the Hall Electron Mobility Gage. The magnitude of mobility in the Mobility Gage was found to be lower than that typically exhibited in a Hall thruster so these findings do not negate the possibility of one or both of these contributing to mobility. However, these findings suggest another mechanism is present driving electron mobility in these fields, separate from both wall collisions and oscillations. The trends of mobility with pressure suggest that collisions do contribute to mobility in the Hall Electron Mobility Gage, showing an increase in mobility with increases in pressure. However, the trends of electron temperature with pressure, combined with the absolute magnitude of mobility, suggest that a collisionless mobility mechanism is also present within the Mobility Gage. The mechanism for mobility in the Hall Electron Mobility Gage has not been identified at this point. Future experiments extending the range of the control parameters will allow greater confidence and resolution of the trends with these parameters.

Appendix

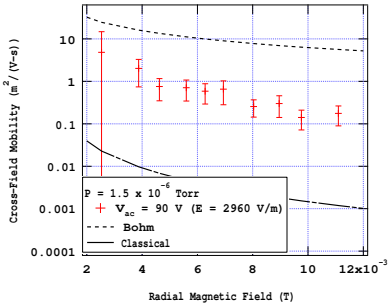

(a) $E = 2960$ V/m; $P = 1.5 \times 10^{-6}$ Torr

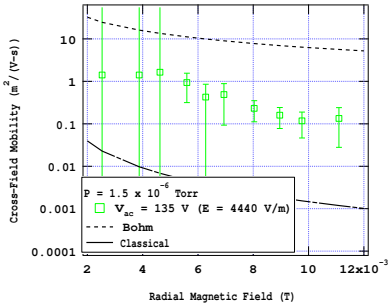

(b) $E = 4440$ V/m; $P = 1.5 \times 10^{-6}$ Torr

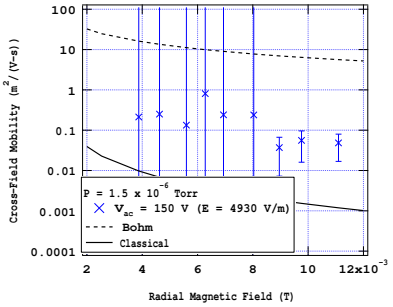

(c) $E = 4930$ V/m; $P = 1.5 \times 10^{-6}$ Torr

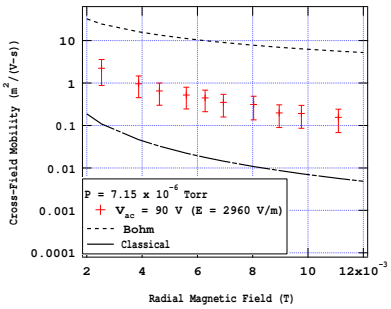

(d) $E = 2960$ V/m; $P = 7.2 \times 10^{-6}$ Torr

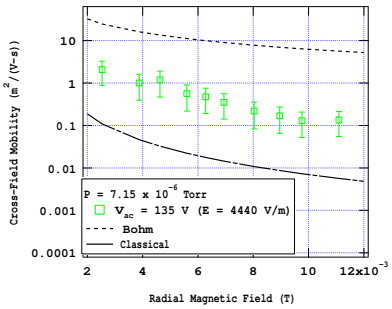

(e) $E = 4440$ V/m; $P = 7.2 \times 10^{-6}$ Torr

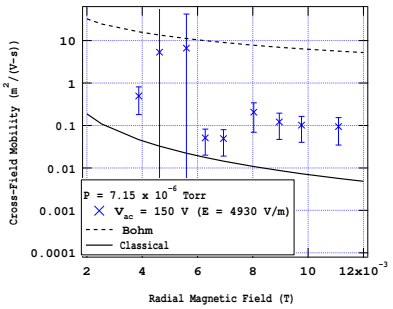

(f) $E = 4930$ V/m; $P = 7.2 \times 10^{-6}$ Torr

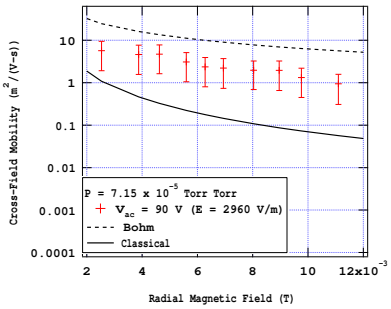

(g) $E = 2960$ V/m; $P = 7.2 \times 10^{-5}$ Torr

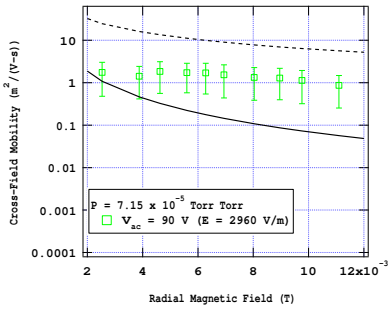

(h) $E = 4440$ V/m; $P = 7.2 \times 10^{-5}$ Torr

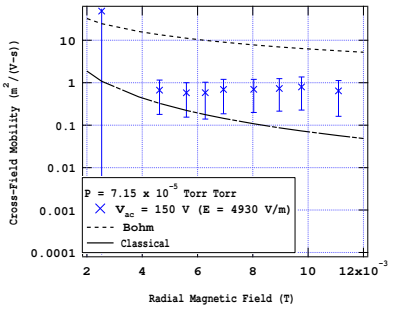

(i) $E = 4930$ V/m; $P = 7.2 \times 10^{-5}$ Torr

Figure 9. Experimental mobility (markers), classical mobility (solid), and Bohm mobility (dashed) versus magnetic field for the conditions of electric field and pressure indicated.

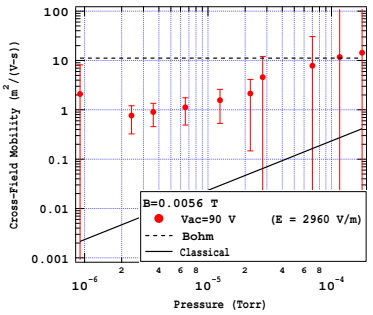

(a) $E = 2960$ V/m; $P = 1.5 \times 10^{-6}$ Torr

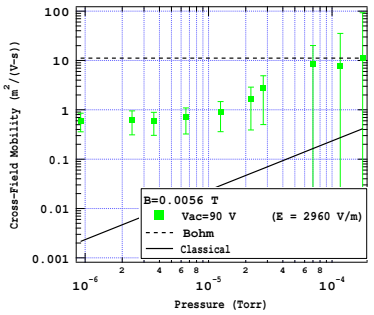

(b) $E = 4440$ V/m; $P = 1.5 \times 10^{-6}$ Torr

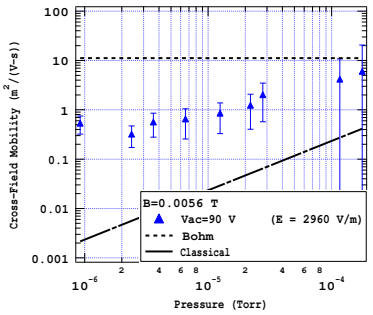

(c) $E = 4930$ V/m; $P = 1.5 \times 10^{-6}$ Torr

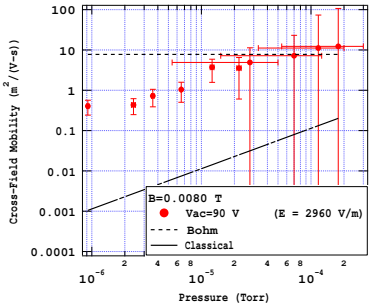

(d) $E = 2960$ V/m; $P = 7.2 \times 10^{-6}$ Torr

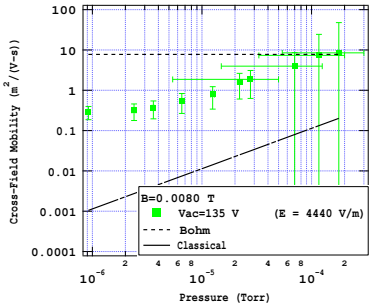

(e) $E = 4440$ V/m; $P = 7.2 \times 10^{-6}$ Torr

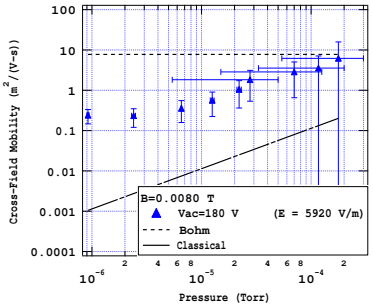

(f) $E = 4930$ V/m; $P = 7.2 \times 10^{-6}$ Torr

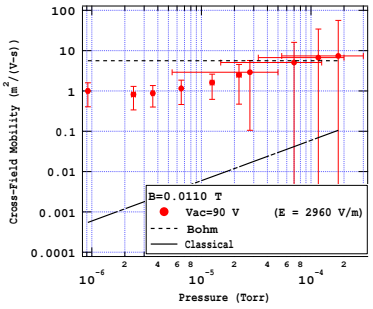

(g) $E = 2960$ V/m; $P = 7.2 \times 10^{-5}$ Torr

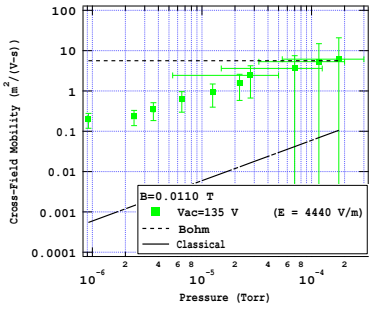

(h) $E = 4440$ V/m; $P = 7.2 \times 10^{-5}$ Torr

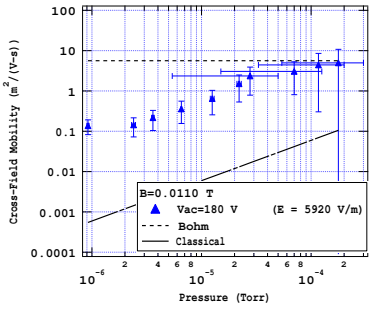

(i) $E = 4930$ V/m; $P = 7.2 \times 10^{-5}$ Torr

Figure 10. Experimental mobility (markers), classical mobility (solid), and Bohm mobility (dashed) versus magnetic field for the conditions of electric field and pressure indicated.

Acknowledgements

The work presented in this manuscript was funded under the National Science Foundation, Grant CBET-0348048.

References

[1] Zhurin, V. V., Kaufman, H. R., and Robinson, R. S., "Physics of closed drift thrusters," *Plasma Sources Sci. Technol.*, Vol. 8, 1999, pp. R1.

[2] Janes, G. S. and Lowder, R. S., "Anomalous Electron Diffusion and Ion Acceleration in a Low-Density Plasma," *Phys. Fluids*, Vol. 9, No. 6, 1966, pp. 1115–1123.

[3] Meezan, N. B., Hargus, W. A., and Cappelli, M. A., "Anomalous electron mobility in a coaxial Hall discharge plasma," *Phys. Rev. E*, Vol. 63, 2001, pp. 026410.

[4] Pote, B. and Tedrake, R., "Performance of a High Specific Impulse Hall Thruster," *27th International Electric Propulsion Conference*, Pasadena, Calif., 15-19 October, 2001, pp. IEPC–2001–35.

[5] Bouchoule, A., Boeuf, J.-P., Heron, A., and Duchemin, O., "Physical investigations and developments of Hall plasma thrusters," *Plasma Phys. Control. Fusion*, Vol. 46, 2004, pp. B407–B421.

[6] Scharfe, M. K., Thomas, C. A., Scharfe, D. B., Gascon, N., Cappelli, M. A., and Fernandez, E., "Shear-Based Model for Electron Transport in 2D Hybrid Hall Thruster Simulations," *43rd AIAA/ASME/SAE/ASEE Joint Propulsion Conference & Exhibit*, Cincinnati, Ohio, 8-11 July, 2007, pp. AIAA–2007–5208.

[7] Cappelli, M. A., Hargus, W. A., and Meezan, N. B., "Coherent Structures in Crossed-Field Closed-Drift Hall Discharges," *IEEE Trans. Plasma Sci.*, Vol. 27, No. 1, 1999, pp. 96–97.

[8] Hofer, R. R., Katz, I., Mikellides, I. G., Goebel, D. M., Jameson, K. K., Sullivan, R. M., and Johnson, L. K., "Efficacy of Electron Mobility Models in Hybrid-PIC Hall Thruster Simulations," *44th Joint Proupulsion Conference & Exhibit*, Hartford, Conn., 21-23 July, 2008, pp. AIAA–2008–4924.

[9] Garrigues, L., Boyd, I. D., and Boeuf, J. P., "Computation of Hall Thruster Performance," *J. Propul. Power*, Vol. 17, No. 4, 2001, pp. 772–779.

[10] Hagelaar, G. J. M., Bareilles, J., Garrigues, L., and Boeuf, J. P., "Role of anomalous electron transport in a stationary plasma thruster simulation," *J. Appl. Phys.*, Vol. 93, No. 1, 2003, pp. 67–75.

[11] Kaganovich, I. D., Raitses, Y., Sydorenko, D., and Smolyakov, A., "Kinetic effects in a Hall thruster discharge," *Phys. Plasmas*, Vol. 14, 2007, pp. 057104.

[12] Raitses, Y., Staack, D., Keidar, M., and Fisch, N. J., "Electron-wall interaction in Hall thrusters," *Phys. Plasmas*, Vol. 12, 2005, pp. 057104.

[13] Meezan, N. B. and Cappelli, M. A., "Kinetic Study of Wall Collisions in a Coaxial Hall Discharge," *Phys. Rev. E*, Vol. 66, 2002, pp. 036401.

[14] Choueiri, E. Y., "Plasma oscillations in Hall thrusters," *Phys. Plasmas*, Vol. 8, No. 4, 2001, pp. 1411.

[15] Knoll, A., Thomas, C. A., Gascon, N., and Cappelli, M. A., "Experimental investigation of high frequency plasma oscillations within hall thrusters," *42nd AIAA/ASME/SAE/ASEE Joint Propulsion Conferene*, Sacramento, California, 2006.

[16] Thomas, C. A., *Anomalous Electron Transport in the Hall-Effect Thruster*, Ph.D. thesis, Stanford University, 2006.

[17] Lazurenko, A., Albarede, L., and Bouchoule, A., "Physical characterization of high-frequency instabilities in Hall thrusters," *Phys. Plasmas*, Vol. 13, No. 8, 2006, pp. 083503.

[18] Lazurenko, A., Dudok De Wit, T., Cavoit, C., Krasnoselskikh, V., Bouchoule, A., and Dudeck, M., "Determination of the electron anomalous mobility through measurements of turbulent magnetic field in Hall thrusters," *Phys. Plasmas*, Vol. 14, 2007, pp. 033504.

[19] Bohm, D., "Chapter 1: Qualitative Description of the Arc Plasma in a Magnetic Field," *The Characteristics of Electrical Discharges in Magnetic Fields;* Chapter 1, edited by A. Guthrie and R. K. Wakerling, McGraw-Hill, New York, 1949, pp. 1–12.

[20] Bohm, D., "Chapter 2: The use of Probes for Plasma Exploration in Strong Magnetic Fields," *Characteristics of Electrical Discharges in Magnetic Fields;* Chapter 2, edited by A. Guthrie and R. K. Wakerling, McGraw-Hill, New York, 1949, pp. 13–76.

[21] Spektor, R., "Quasi-Linear Analysis of Anomalous Electron Mobiltiy Inside a Hall Thruster," *30th International Electric Propulsion Conference*, Florence, Italy, 17-20 Septemver, 2007, pp. IEPC–2007–70.

[22] Fernandez, E., Scharfe, M. K., Thomas, C. A., Gascon, N., and Cappelli, M. A., "Growth of resistive instabilities in ExB plasma discharge simulations," *Phys. Plasmas*, Vol. 15, No. 1, 2008, pp. 012102.

[23] Levchenko, I., Keidar, M., and Ostrikov, K., "Electron transport across magnetic field in low-temperature plasmas: An alternative approach for obtaining evidence of Bohm mechanism," *Phys. Lett. A*, Vol. 373, 2009, pp. 1140–1143.

[24] Keidar, M. and Brieda, L., "Modeling electron transport within the framework of hydrodynamic description of Hall thrusters," *44th AIAA/ASME/SAE/ASEE Joint Propulsion Conference & Exhibit*, Hartford, CT, 21-23 July, 2008, pp. AIAA–2008–5186.

[25] Fossum, E. C. and King, L. B., "Confinement time in an electron trap used for electron mobiltiy studies in Hall thruster-like fields," *30th International Electric Propulsion Conference*, Florence, Italy, 2007, p. 153.

[26] Pines, D. and Bohm, D., "A Collective Description of Electron Interactions: II. Collective vs Individual Particle Aspects of the Interactions," *Phys. Rev.*, Vol. 85, No. 2, 1952, pp. 338.

[27] Fossum, E. C. and King, L. B., "An electron trap for studying cross-field mobility in Hall thrusters," *IEEE Trans. Plasma Sci.*, Vol. 36, No. 1, 2008, pp. 2088.

[28] Fossum, E. C., *Electron Transport in ExB Devices*, Ph.D. thesis, Michigan Technological University, 2009.

[29] "http://www.ansoft.com/maxwellsv/," .

[30] CPAT and Kinema Software. 1 June 2009, "The Siglo Database, http://www.siglo-kinema.com," .

[31] Gombosi, T. I., *Gaskinetic Theory*, Cambridge University Press, 1994.

[32] Grissom, J. T., Compton, R. N., and Garrett, W. R., "Slow Electrons from Electron-Impact Ionization of He, Ne, and Ar," *Phys. Rev. A*, Vol. 6, No. 3, 1972, pp. 977.